university of groningen

faculty of science and engineering

Comparison of the $\Lambda_b^0 \to \Lambda^0 J/\psi$ and $\overline{\Lambda}_b^0 \to \overline{\Lambda}^0 J/\psi$ decays at the LHCb experiment

Author: Laura Vasiliauskaite (s4257065)

Supervisor: Dr. Ann-Kathrin Perrevoort
Second examiner: Dr. Daan van Eijk

Bachelor Thesis - September 25, 2024

Abstract

The goal of this research is to analyze the $\Lambda_b^0 \to \Lambda^0 J/\psi$ and the $\overline{\Lambda}_b^0 \to \overline{\Lambda}^0 J/\psi$ decays at the LHCb experiment, to test matter-antimatter symmetry. The presence of asymmetry in the ratio of the particle and antiparticle counts could suggest the presence of CP violation effects, which are one avenue of research when investigating physics beyond the Standard Model. The data analysis was conducted on the Run 2 data (years 2016 to 2018), using proton-proton collisions at 13 TeV with a luminosity of 5.4 fb^{-1}. The particle-antiparticle ratio was determined to be $2.0 \pm 1.5\%$, which is not statistically significant, meaning that no asymmetry was observed. Subsequently, this means that no CP violation effects were detected.

Acknowledgments

I would like to thank my supervisor Ann-Kathrin Perrevoort, who guided me through the entire process of my bachelor's thesis with grace and efficiency. Thank you for all the late-hour replies and quick reactions and especially thank you for all your help with the data fitting process. Furthermore, I would like to thank the entire LHCb Groningen group, who accepted me so warmly, helped me whenever I asked for help, and even sat through my entire thesis presentation twice, once for practice and once for the official version.

Contents

1. Introduction

The study of science is the accumulated body of knowledge about Nature, built through generations of testing, retesting, and revision by people from all around the world. It stems from the innately human curiosity and desire to understand the natural world and the laws that govern it. Physics, by its very name, focuses on the physical aspects of nature, seeking to understand that which governs the properties and behavior of matter. As the scope of matter and phenomena under investigation broadened over time, the field of physics itself expanded significantly throughout the century [10]. The field of particle physics first arose at the turn of the 20th century, when in 1925, Max Born coined the term "quantum mechanics" for the very first time [11]. From there on, other well-known names in the field such as Heisenberg, Jordan, Schrödinger and Dirac formalized the quantum mechanics as a proper field of study which propelled humanity into a new age of discovery going far beyond the scale of what is observable.

Skipping forward by a couple of decades, at the end of World War 2, more specifically in 1952, the European Council for Nuclear Research, better known by its acronym CERN, was established [9]. With the rise of new technologies enabling the testing of previously only theorized phenomena, the field of particle physics truly came into itself. So far, it has led to a plethora of discoveries, all culminating in the theory of the Standard Model (SM) which, to date, is the best theory available to describe the most fundamental particles and their interactions. Unfortunately, this model is still incomplete. Phenomena such as gravity, Dark Matter, and the asymmetry in the abundance of matter and antimatter in the Universe still to this day puzzle particle physicists on their place in the theory.

One avenue of exploration to search for new physics beyond the SM is to look for CP symmetry violation (CPV), where C is the charge-conjugation operator and P is the parity operator. This is also one of the three Sakharov criteria that describe the necessary conditions for baryogenesis, the process that creates matter-antimatter asymmetry in the Universe [16]. CPV is accounted for in the SM, however, it is not sufficient to explain the asymmetry in the abundance of matter and antimatter in the Universe, this is why further investigations into CPV are needed. To fully unravel this mystery, however, all three of the Sakharov criteria [16] must be studied.

The current theory does not offer sufficient explanation for the preponderance of matter in the Universe [4]. For that reason, the LHCb Collaboration at CERN has been investigating the properties of hadronic decays and comparing them to the theoretical SM predictions to solve the conundrum of matter-antimatter asymmetry [13]. One type of such decay of interest is the b-hadron decay. Initially, CP violation was discovered in neutral K meson decays and further observed in B meson decays [4]. Since in both cases mesons were involved, it is now of interest to look at baryonic decays as well. The decay of the Λ_b^0 baryon to final states consisting of baryons without the charm quark in particular look to be promising, as they are predicted

to have CP violations as large as 20% for specific decay modes [4]. Investigating these decays is one of the more promising ways to currently test the limits of the SM and see what extensions are to follow.

The $\Lambda_b^0 \to \Lambda^0 ll$ with $l = e, \mu, \tau$ decay is a good candidate for the type of b-hadron decays mentioned above. This decay can further be split into several decays to be analyzed based on the leptons produced in the final states. Most commonly, these leptons are either electrons or muons. Here, the final states involving muons are the focus, given that they usually have better resolution and are not affected as strongly by bremsstrahlung effects. However, before this decay can be studied, all of its possible decay channels must be fully known. Thus, in this research, one such decay channel, the $\Lambda_b^0 \to \Lambda^0 J/\psi(\to \mu^+\mu^-)$ decay, is examined, where an intermediate $c\bar{c}$ resonance (the J/ψ) is produced and then decays to a dimuon pair.

To conclude, this paper will provide a brief overview of the Standard Model theory, discuss CPV and its effects in the context of the weak interaction, and finally focus on the analysis of the $\Lambda_b^0 \to \Lambda^0 J/\psi(\to \mu^+\mu^-)$ decay (as well as its antiparticle version) in order to confirm the presence of CPV and as a result, discuss particle-antiparticle symmetry. The analysis process will be conducted on Run 2 data (proton-proton collisions at LHCb, taking years 2016 to 2018 with energy of 13 TeV and luminosity of 5.4 fb^{-1}) and will separately analyze the Λ_b^0 as well as its antiparticle counterpart.

2. Theory

2.1 The Standard Model

The Standard Model (SM) of particle physics is a theoretical framework that describes the sum of all our knowledge of the fundamental particles and the forces that govern them, except gravity. It is a quantum theory that is part of the specific field of quantum field theory and so far, it has been very successful in describing all known particles and their interactions. There are two types of fundamental particles in the SM: fermions and bosons.

Fermions are particles that are the building blocks of matter and antimatter. They follow Pauli's exclusion principle and are half-integer spin particles (e.g. spin 1/2). Fermions are further divided into two types, quarks and leptons, that each come in three generations of doublets. Quarks are classified into up-type and down-type flavours within the three generations as follows: up (u) and down (d); charm (c) and strange (s); top (t) and bottom (b). The last generation quarks are also sometimes named truth (t) and beauty (b). Quarks combine to form hadrons that consist of a quark-antiquark pair (known as a meson) or a combination of three quarks (known as a baryon). The most commonly known hadrons are protons and neutrons which are both examples of baryons. Similarly to quarks, the three generations of leptons also come in pairs and are classified as follows: electron (e^-) and electron neutrino (ν_e); muon (μ^-) and muon neutrino (ν_μ); tau (τ^-) and tau neutrino (ν_τ). All six quarks and all six leptons have antiparticles that have the same mass but opposite quantum numbers and charge, except for neutrinos which do not carry charge. Counting the particles and antiparticles results in 24 fundamental fermions.

Within the SM, the second type of particle is known as a boson. This type of particle is referred to as a "force-carrier" or a gauge boson and it is responsible for the different types of interactions between fermions. Bosons are integer-spin particles (e.g. spin 1) and form fields known as boson fields through which the interactions are mediated as follows: massless photons (γ) that mediate the electromagnetic interaction between charged particles; massive W^+, W^-, Z bosons that mediate the weak interaction between particles with flavour (i.e. leptons and quarks); massless gluons (g) that mediate the strong interaction between particles that have colour charge (i.e. quarks). In addition to this, there is also the massive scalar Higgs boson through which massive fermions and bosons acquire their mass. To sum up, all the fundamental particles contained within the SM are schematically represented in Fig. 2.1.

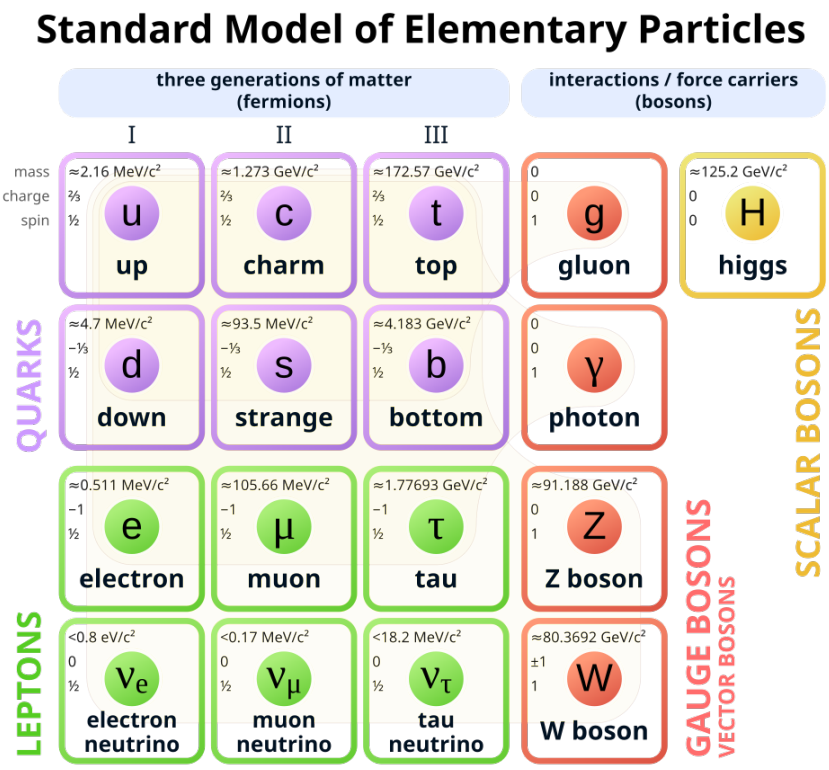

Figure 2.1: The fundamental Standard Model particles and their properties [3].

Unfortunately, there are still some things that lie outside the SM such as gravity, dark matter dark energy and lastly neutrino masses. Although research is currently being conducted in these fields, it is still likely going to be a little while before any new contributions are added to the SM.

2.2 The weak interaction and CP violation

The weak interaction is the only interaction known that allows for the violation of certain conservation laws, such as the parity (P), the combined charge, and parity symmetry (CP) as well as the changing of quark and lepton flavours in specific decays. The most important conservation laws violated to consider in this paper, are the CP and the conservation of quark flavour, where C and P are the charge-conjugation and parity operators respectively. In particle physics, CP violation (CPV) is the breaking of charge-parity symmetry, which states that the laws of physics remain invariant if particles are switched with their antiparticles (C symmetry) and left and right directions are reversed (P symmetry). Within the SM, CPV is accounted for by the Cabibbo-Kobayashi-Maskawa (CKM) mechanism which describes the mixing of the up- and down-type quarks [5] [6] through the emission of a virtual W boson and changing of sign in the phases of the couplings between quarks

and antiquarks. Despite this, the amount of CPV predicted in the CKM mechanism is not enough to explain the matter-antimatter asymmetry in the Universe and so further sources of CPV are necessary [4].

The decay studied in this paper is the $\Lambda_b^0 \to \Lambda^0 J/\psi(\to \mu^+\mu^-)$, which is mediated by the weak interaction and is described on the quark-level by the $b \to s$ transition. This is a rare decay which is of particular interest when studying CPV since it is one of the decay channels of the $\Lambda_b^0 \to \Lambda^0\mu^+\mu^-$ decay, predicted to have non-negligible CP asymmetry[4]. The $\Lambda_b^0 \to \Lambda^0\mu^+\mu^-$ decay is highly important as this decay involves flavour changes while remaining neutral in charge which is not allowed on the tree-level diagrams in the SM and can only happen in higher order diagrams, specifically the electroweak loop (also known as the penguin and W box) diagrams [14].

2.3 The Λ_b^0 decay

There are a variety of paths to explore that have the potential to lead beyond the SM and into the territory of new physics (NP). Of these, flavour physics is one such key area. In the flavour physics sector, rare decays are particularly suitable for investigating physics beyond the SM. From these, decays involving the $b \to s(d)$ transition are particularly attractive, as they are not allowed in the tree-level diagrams and occur only at loop level. So far, rare decays of the B meson have been studied in detail both theoretically and experimentally [19]. To find traces of NP, decays involving this particle have been extensively researched within the context of numerous NP models that exist in literature (e.g. extra-dimension models, supersymmetric models, etc.) [19]. Presently, the focus is shifting more towards the baryonic sector, specifically the Λ_b baryon.

The first decay of interest in this research is $\Lambda_b^0 \to \mu^+\mu^-$, which is a rare flavour-changing $b \to s$ neutral current decay. It proceeds through an electroweak loop, also known as a penguin and $W^\pm$ box, which is a higher order diagram shown in Figure 2.2. Due to the potential contribution of non-SM particles in the decay amplitudes, measuring this and similar decays is one possible avenue to search for physics beyond the SM [14].

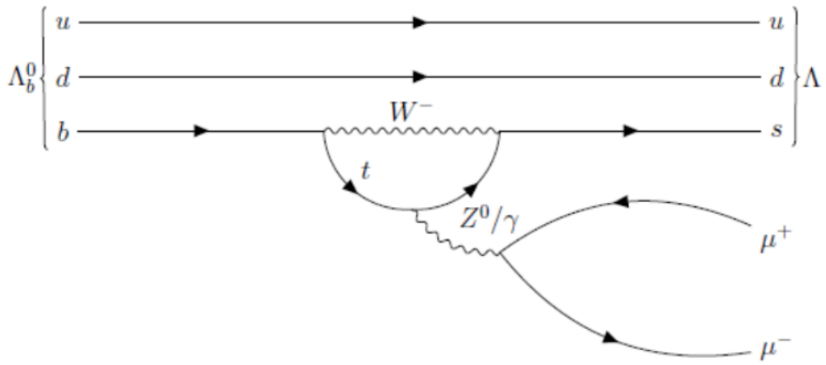

Figure 2.2: The penguin diagram of the $\Lambda_b^0 \to \Lambda^0 \mu^+ \mu^-$ decay taken from [17].

There are, however, some issues when attempting to analyze this decay, since it is very rare and is currently not well explored. Due to this, similar decay modes that have the same final states are used to build up knowledge. One such decay is the $\Lambda_b^0 \to \Lambda^0(\to p^+\pi^-)J/\psi(\to \mu^+\mu^-)$ decay mode (Fig. 2.3).

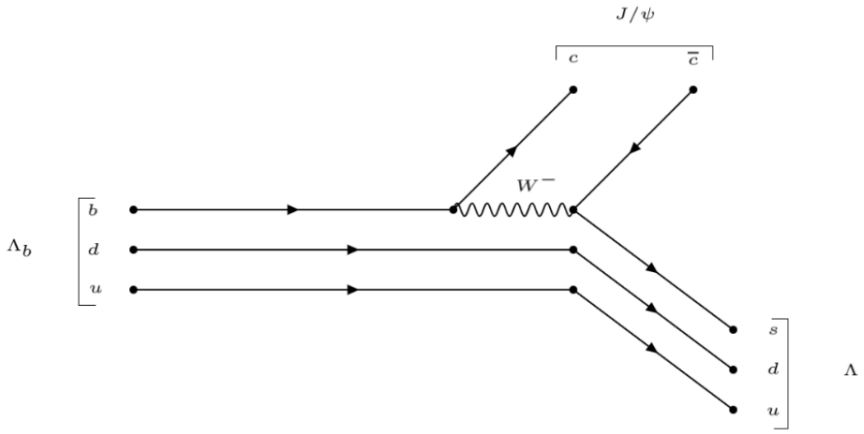

Figure 2.3: The tree level diagram of the $\Lambda_b^0 \to \Lambda^0 J/\psi$ decay taken from [17]

Here, the final state with a Λ^0 particle as well as two muons is the same, however, it holds several distinct advantages. Firstly, this decay is less rare, thus alleviating the analysis process (a comparison of the branching fractions is shown in Table 2.1). Secondly, the secondary $\Lambda^0 \to p^+\pi^-$ decay proceeds the same way as in the $\Lambda_b^0 \to \Lambda^0 \mu^+ \mu^-$ decay and lends itself well to differentiating the Λ^0 and the $\overline{\Lambda}^0$ particles, thus leading to a calculable ratio to compare matter-antimatter symmetry.

Decay mode	Branching fraction	q^2 region
$\Lambda_b^0 \to \Lambda J/\psi$	$(3.08 \pm 0.26) \cdot 10^{-4}$	-
$\Lambda_b^0 \to \mu^+\mu^-$	$(7.1 \pm 2.7) \cdot 10^{-8}$	$q^2 < 2.0\ GeV^2/c^4$

Table 2.1: The two relevant decay modes as well as their branching fractions as taken from [7][18] respectively

Consequently, the focus of this research is the $\Lambda_b^0 \to \Lambda^0 J/\psi(\to \mu^+\mu^-)$ decay which is then used to determine the symmetry between the Λ^0 and $\overline{\Lambda}^0$ count and from there to further draw conclusions on the symmetry between matter and antimatter.

Zooming out to look at the overall decay chain of the decay to be analysed, Figure 2.4 displays a graphical representation of the $\Lambda_b^0 \to \Lambda^0 J/\psi$ decay topology. Here, the black arrows represent the particles measured by the detector and the purple arrows represent the particles that are reconstructed to form the full decay tree.

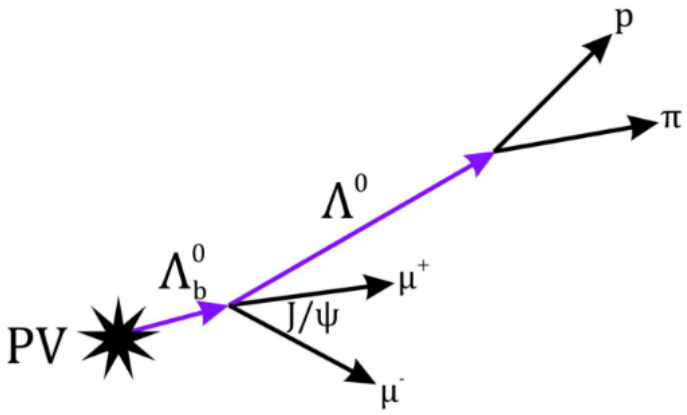

Figure 2.4: A graphical representation of the $\Lambda_b^0 \to \Lambda^0 J/\psi$ decay topology

Furthermore, Table 2.2 displays the properties of all the particles involved in the decay represented above. Here, the most important information to consider is the quark composition of the particles involved (to better understand the Feynman diagrams) as well as the mass of the Λ_b^0 particle, as it will become relevant later on.

Particle	Quark content	Mass (MeV)	Charge
Λ_b^0	udb	5619.60 ± 0.17	0
Λ	uds	1115.683 ± 0.006	0
J/ψ	$c\overline{c}$	3096.900 ± 0.006	0
μ	-	$105.6583755 \pm 0.0000023$	-
proton	uud	$938.27208816 \pm 0.00000029$	+
π	$u\overline{d}$	139.57039 ± 0.00018	-

Table 2.2: The properties of the particles involved in the decay, taken from [7] (uses natural units)

3. The LHC and the LHCb

The Large Hadron Collider (LHC), located in Geneva Switzerland, is the largest and most powerful particle accelerator in the world. It first began operations on 10 September 2008 and is the most recent addition to CERN's accelerator complex. The LHC features a 27-kilometer ring of superconducting magnets along which there are accelerating structures that increase the energy of particles as they travel through the collider [8].

The controls for the accelerator, along with its services and technical infrastructure, are centralized at the CERN Control Centre. From this location, the particle beams in the LHC are directed to collide at four different stations along the accelerator ring, where the four particle detectors—ATLAS, CMS, ALICE, and LHCb—are positioned [8].

LHCb is an experiment focused on heavy flavor physics at the LHC. Its main objective is to search for indirect signs of new physics by studying CP violation and (rare) decays of beauty and charm hadrons.

The LHC has operated in several phases. Run 1 took place from 2010 to 2012 with a collision energy of $\sqrt{s} = 7$ TeV, while Run 2 ran from 2015 to 2018 at $\sqrt{s} = 13$ TeV. Run 3 started in July 2022, with collisions occurring at $\sqrt{s} = 13.6$ TeV. In Run 2, LHCb generated about 1 TB of data per second, a volume too large to store in its entirety. To manage this, various data reduction methods are employed without compromising quality.

3.1 The LHCb detector

The LHCb detector is a single-arm spectrometer with forward angular coverage, optimized for studying the production of b- and $\bar{b}$-hadrons at high energies, where these particles are generated predominantly in the forward or backward directions. It operates with an acceptance in the pseudorapidity range of $2 < \eta < 5$ [12]. The LHCb experiment is located at Intersection Point 8 of the LHC, previously used by the DELPHI experiment, with modifications to the LHC optics to accommodate the detector.

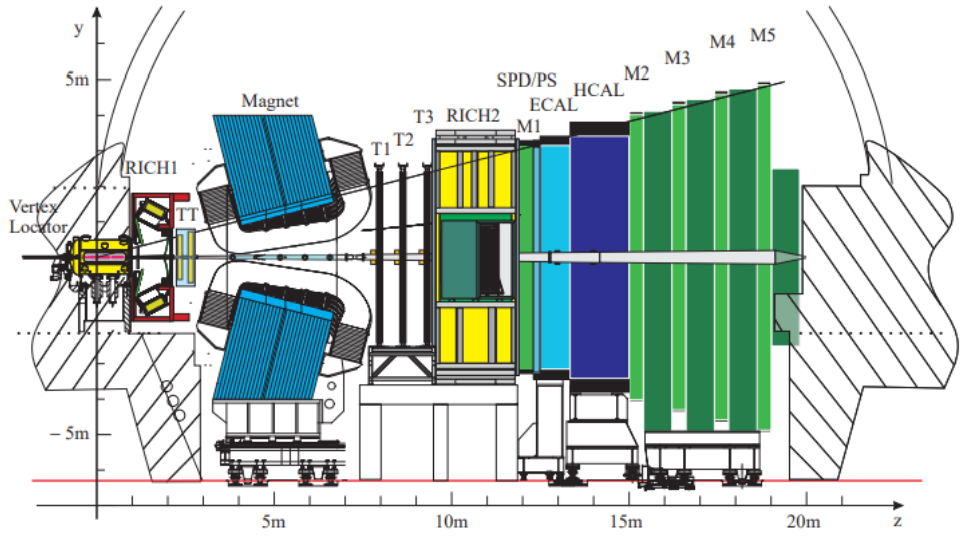

Figure 3.1: The schematics of the LHCb detector [21]

The main components of the detector, as seen above in Figure 3.1, are thusly enumerated: the spectrometer magnet which is a warm dipole magnet providing an integrated field of 4 Tm; the vertex locator system (VELO), which includes a pile-up veto counter; the tracking system, consisting of the Trigger Tracker (a silicon microstrip detector, TT) in front of the spectrometer magnet and three tracking stations behind it using silicon microstrips in the inner parts and Kapton/Al straws in the outer parts (T1, T2, T3); the two Ring Imaging Cherenkov counters (RICH1 and RICH2), which use Aerogel, C4F10, and CF4 as radiators to provide excellent $\pi - K$ separation in the momentum range of 2 to 100 GeV/c, along with Hybrid Photon Detectors; the calorimeter system, comprising a Scintillator Pad Detector and Preshower (SPD/PS), an electromagnetic calorimeter (ECAL), and a hadronic calorimeter (HCAL); the muon detection system (M1-M5), which primarily uses multi-wire proportional chambers (MWPC), except in high-rate areas where triple-GEMs are employed [20].

During the upgrade of the detector between the years 2013 and 2016, the LHCb trigger system was redesigned to perform the full reconstruction of offline events, allowing for real-time detector alignment, calibration, and analysis using trigger system data. The two key objectives of this overhaul were as follows: enabling full offline reconstruction within the trigger, allowing for increased efficiency in selecting charm- and strange-hadronic decays; matching the trigger alignment and calibration quality as was achieved in Run 1 offline, facilitating the final signal selection at the trigger level [12].

Lastly, the LHCb detector has two settings for measuring data, magnet up (MU) and magnet down (MD), which are especially relevant as they are necessary to test the symmetry of the data gathered to comprehensively analyze the $\Lambda_b^0 \to \Lambda^0 J/\psi(\to$

$\mu^+\mu^-$) decay. Furthermore, the particles detected for this research can be differentiated by the track type, i.e., long track or downstream track. The differences between these two track types are illustrated in the figure below (Fig. 3.2).

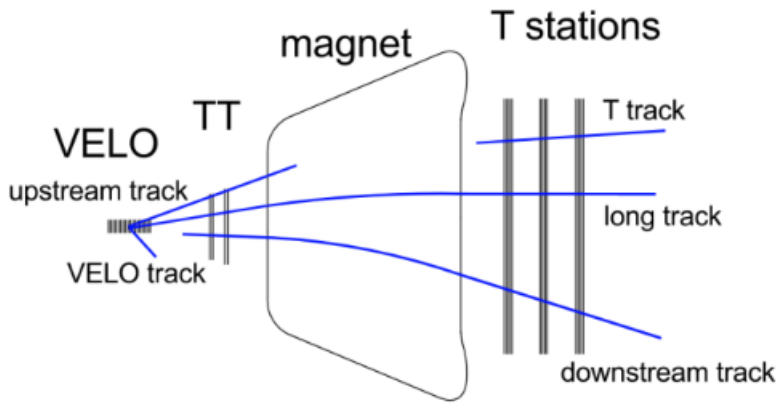

Figure 3.2: A schematic drawing of the different track types and the VELO in the detector [18]

For the purposes of the data analysis process, the type of particle track is not differentiated, long and downstream track particle candidates are analyzed as one cohesive dataset.

4. Analysis and Results

The analysis is conducted using Python [1] in combination with the uproot [2] package which allows for the retrieval as well as the detailed processing of the data collected at the LHCb detector. The uproot library in Python is specifically designed to be compatible with the data format used by CERN. The other alternative is using ROOT directly, which is the primary software package used at CERN and is therefore the format in which the data is processed after collection. Indeed, some of the parameters of the fit functions for the peaking background and the focal Λ_b^0 mass peak were first calculated in ROOT and then loaded into uproot. The data used in the subsequent analysis is taken from Run 2, specifically the years 2016 to 2018, using p-p collisions at 13 TeV with a luminosity of 5.4 fb^{-1} for the years specified.

Although data collected during the year 2015 is also part of Run 2, the data from this year was neglected due to there being some trigger lines that were not available before 2016. Furthermore, the exclusion of the 2015 data is not a big detriment (reduces data by about 5%), the results of the data analysis will not be affected and will be more viable since all the parameters and resolutions remain the same throughout all the data sets compiled from the rest of the Run 2 years. Lastly, all of the analysis conducted combines both MU and MD as well as long and downstream track candidates. Since the goal of this paper is to analyze the particle-antiparticle symmetry, there is no need to specifically differentiate between the different types of candidates due to the final result being a ratio.

Lastly, note that the following analysis is done and presented assuming natural units (i.e. $c = \hbar = 1$).

4.1 Selection rules for Λ_b^0 candidates

In order to select appropriate Λ_b^0 candidates, the first step is to apply the selection rule that naturally arises from the configurations of the LHCb detector. One of the features of this detector, as mentioned before, is that it operates with the acceptance in the pseudorapidity range $2 < \eta < 5$ [12]. Due to this, the first selection rule to be applied concerns the Λ_η variable being restricted to be in the open range $(2, 5)$.

The next step is to analyze the simulated data and from there, determine selection rules as well as the relevant ranges to narrow down the amount of data to be analyzed as well as clearly distinguish the features of the signal. The simulations used for this purpose are produced using the Monte Carlo method, which simulates the decay of the Λ_b^0 particle as well as the further decays from the particles produced, the interaction of particles, and the detector response. This is then reconstructed like real data. Unfortunately, there are no simulations for the combinatorial background, background decays are simulated individually. In this way, using the uproot library, the decay tree of the following decay is selected:

$$\Lambda_b^0 \to \Lambda^0 J/\psi \tag{4.1}$$

The variables that are of interest here are the invariant dimuon mass squared q^2 and the mass of the Λ_b^0 particle. The q^2 is an important variable, as it represents the square of the invariant mass of a system containing two muons, and plays a key role in identifying the presence of specific particles which decay into two muons (i.e. the Z boson). By specifying a q^2 range, the data can be screened for different resonances, in this case, to select the J/ψ resonance.

From the plot of the q^2 variable, an appropriate range of $(8, 11)$ MeV is selected through fully encapsulating the main peak, including the tails of the distribution to either side as shown in Figure 4.1.

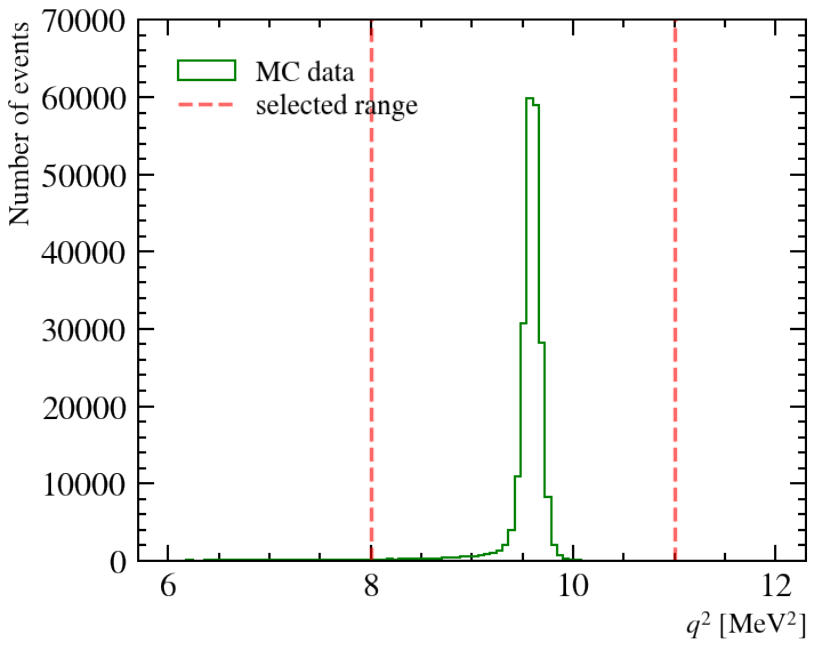

Figure 4.1: Plotting the squared dimuon mass q^2 from simulated data for Λ_b^0 in order to select the J/ψ resonance.

The range for this variable is easily determined since the data used is simulated and therefore the width of the whole distribution is easily contained within the selected range. On top of that, the decay involves muons which means that the resolution of the data is very high, and therefore statistical measures are not necessary to achieve a satisfactory q^2 range.The determined q^2 range is the second of the selection rules to be later applied to the Λ_b^0 mass plots.

In addition to the above-determined selection rules, is it also important to consider the theoretically determined masses of the particles involved in the decay. Restrictions are placed on the mass of the Λ_b^0 particle especially, since selecting the correct plotting range is necessary to avoid confusion with the shape of the combinatorial

background when analyzing the real data. For this reason, the masses and other relevant properties of the particles involved are recalled from table 2.2 in section 2.3. From this table, the plotting range for the Λ_b^0 mass is taken to be $(5000, 6000)$ MeV.

Lastly, it is important to note, that the variable selected to plot the mass of the Λ_b^0 particle is first processed by the decay tree fitter (DFT). Here, the DFT is used to reconstruct the entire decay chain from the final state particles while fixing the masses of the intermediate Λ^0 and J/ψ particles to literature values. This difference is important since the fitted mass variable produces clearer plots that are easier to analyze. Although using the unfitted mass variable will also achieve the same results, the resolution will not be as high and the fitting procedures will have an enhanced level of difficulty.

Following all of the above-mentioned procedures and applying all of the selections as determined from the Monte Carlo simulations to the real data, results in the plot of the Λ_b^0 mass as shown in Figure 4.2.

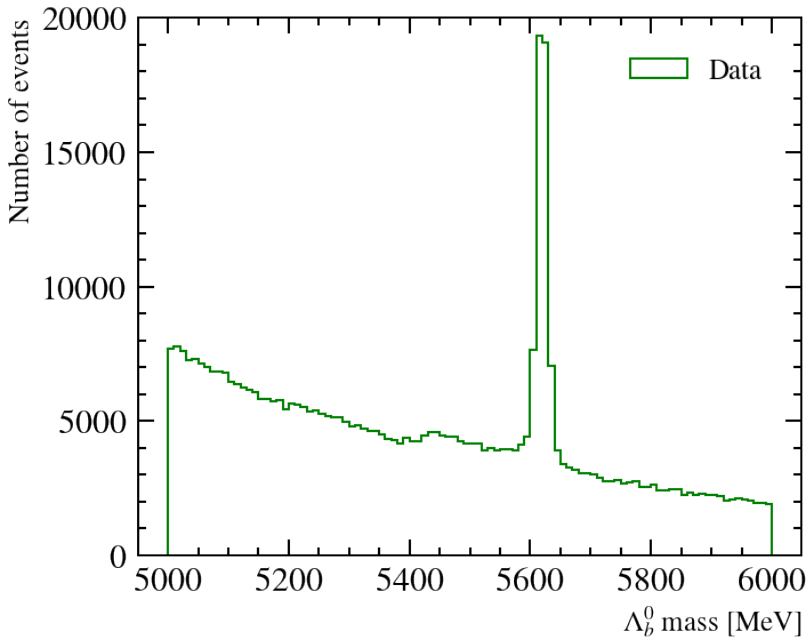

Figure 4.2: Plotting the mass of the Λ_b^0 particle using real data

Figure 4.2 shows the real data with a peak for the Λ_b^0 mass at slightly higher than 5600 MeV, which matches the literature value (seen in Table 2.2). On top of that, there is a very clear background, composed of two parts: the combinatorial background as well as an additional broad peak left of the Λ_b^0 mass peak. Arising from other stray particles detected in the detector, the combinatorial background takes the shape of a smooth slope, decreasing from left to right on the selected range. However, as can be seen from Figure 4.2, left of the main peak of the Λ_b^0 particle mass, there is a broad peak around the $(5400, 5550)$ MeV range which is part of the

background, but does not fit the expected combinatorial background shape, hence it must originate from a different source. Indeed, this discrepancy in the background arises from another decay and is referred to as the peaking background henceforth. Since the peaking background mimics the signal, there is a need to differentiate between the signal and it. This differentiation can be approached in several ways.

The first and the easiest would be to restrict the range such that the peaking background does not affect the main peak of the plot. This approach, however, is somewhat negligent of the signal and if the range is not restricted in a systematic way, can lead to major losses in the signal to be analyzed. Furthermore, leaving the peaking background within the further data analysis could detrimentally affect the credibility of the particle-antiparticle ratio calculation, as there would be more variables inter-playing, the effects of which would be difficult to account for. The second approach is to either fit the peaking background separately or eliminate it wholly. For the purposes of this paper, the approach selected is to make a cut such that the peaking background is reduced as much as possible while maintaining a high signal efficiency. The process through which this is done is described in the following section.

4.2 Peaking background

The only relevant contribution to be considered when studying the $\Lambda_b^0 \to \Lambda^0 J/\psi$ decay channel comes from the $B^0 \to J/\psi K_s^0$ decay, where $K_s^0 \to \pi^+\pi^-$ with one of the pions being misidentified as a proton [14]. This decay contains a K_s^0 meson with a long lifetime (i.e. longer than usual) which results in a similar topology as the $\Lambda_b^0 \to \Lambda^0 J/\psi$ decay. This contribution results in a broad bump shape that peaks below the Λ_b^0 mass region [14]. To eliminate this broad peak from the Λ_b^0 mass plot, it is first important to analyze it using the Monte Carlo simulations. The cut to be applied is on the mass of the K_s^0 particle, thus the best mass range on which to cut needs to be determined.

The equation to calculate the K_s^0 mass is taken fully derived, however, the derivation process is not difficult to follow and combines the simple equations shown in 4.2. Here E indicates energy and p indicates momentum with appropriate subscripts indicating the particle they belong to.

$$\begin{aligned} \text{mass} &= \sqrt{E^2 - p^2} \\ \text{with } E &= E_p + E_\pi \\ p &= p_p + p_\pi \end{aligned} \tag{4.2}$$

From there, equation 4.3 [15] follows and is then used in order to determine the mass of the K_s^0 particle:

$$m_{K_s^0} = \sqrt{\left(E_\pi + \sqrt{m_{\pi^0}^2 + |\vec{P}_p|^2)}\right)^2 - (\vec{p_\pi} + \vec{p_p})^2} \tag{4.3}$$

In this equation, the subscripts indicate the variable and are specified according to the particle: E_π is the total energy of the pion; m_{π^0} is the rest mass of the pion; $\vec{P_p}$ is the total momentum of the proton; $\vec{p_\pi}$ and $\vec{p_p}$ are the x, y, z components of the pion and proton respectively.

For the use of this equation, it is important to note that here, the values of the energy and momentum of the pions and protons are used as measured for the $\Lambda^0 \to p^+\pi^-$ decay, however, the rest mass of the proton is exchanged for a pion to reconstruct the $K_s^0 \to \pi^+\pi^-$ decay within the context of the peaking background.

After applying Equation 4.3 on the simulated data, an appropriate selection in $m_{K_s^0}$ which encompasses the peaking background but does not hurt the signal must be determined. This process is carried out statistically, by first determining the mean ($\mu_{K_s^0}$) and the standard deviation ($\sigma_{K_s^0}$) of the K_s^0 mass peak and then based on those results, in multiples of $\sigma_{K_s^0}$ around $\mu_{K_s^0}$, the events are excluded in this range until a satisfactory signal efficiency versus background efficiency is achieved. To improve these efficiencies further, the range is then manually adjusted.

The signal efficiency is calculated by taking the ratio in Equation 4.4 which is then converted into a percentage. Here, N_{sig}^{sel} denotes the signal selected and N_{sig}^{tot} denoted the total signal.

$$\epsilon_{sig}^{sel} = \frac{N_{sig}^{sel}}{N_{sig}^{tot}} \tag{4.4}$$

The background efficiency is similarly calculated by finding the ratio in Equation 4.5 which is also converted into a percentage. As above, N_{bck}^{sel} denotes the background selected and N_{bck}^{tot} denoted the total background.

$$\epsilon_{bck}^{sel} = \frac{N_{bck}^{sel}}{N_{bck}^{tot}} \tag{4.5}$$

By tuning these two percentages and optimizing the ratios such that the signal efficiency is maximized whereas the background efficiency is minimized several ranges are determined and shown in table 4.1. From these ranges, the $(480, 515)$ MeV range is selected for the K_s^0 mass cut.

Cut range [MeV]	Signal efficiency	Background efficiency
$(480, 515)$	82.33%	3.37%
$(480, 512)$	84.01%	4.36%
$(480, 518)$	80.69%	2.91%
$(490, 510)$	90.86%	13.98%

Table 4.1: The different tested ranges of the K_s^0 mass cut with their respective signal and background efficiency values with selections applied.

Moving forward, the K_s^0 mass cut is then applied to the real data to eliminate the bump in the Λ_b^0 mass plot. The result of applying this cut is shown in Figure 4.3.

From the plot is it easy to determine by eye that the peaking background has vanished, leaving only a smooth combinatorial background which is then fitted according to the procedures discussed in the next section.

Finally, all the selections made can now be summarized, as shown in Table 4.2.

Variable	Selection	Reason
η	$(2, 5)$	detector specification
q^2	$(8, 11)$ MeV^2	J/ψ resonance selection
$m_{\Lambda_b^0}$	$(5000, 6000)$ MeV range	plotting clarity
$m_{K_s^0}$	$(480, 515)$ MeV cut	eliminating peaking background

Table 4.2: The summary of all the selections that are henceforth applied to the data being analyzed.

4.3 Combinatorial background

The combinatorial background arises from random combinations of particles. In this paper, it is parametrized using an exponential function [14] before and after the Λ_b^0 mass peak separately to determine the best-fit parameters for both segments and then combined into one cohesive fit.

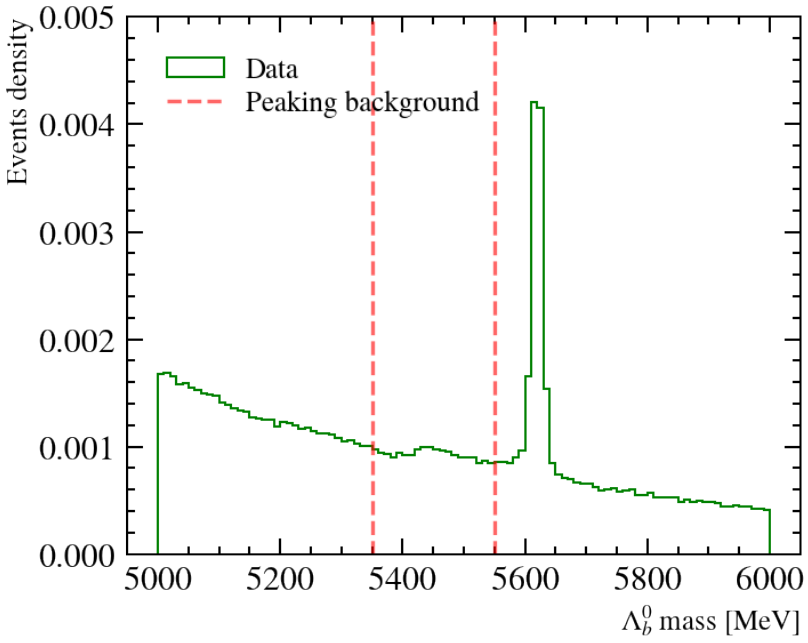

(a) Without peaking background cut

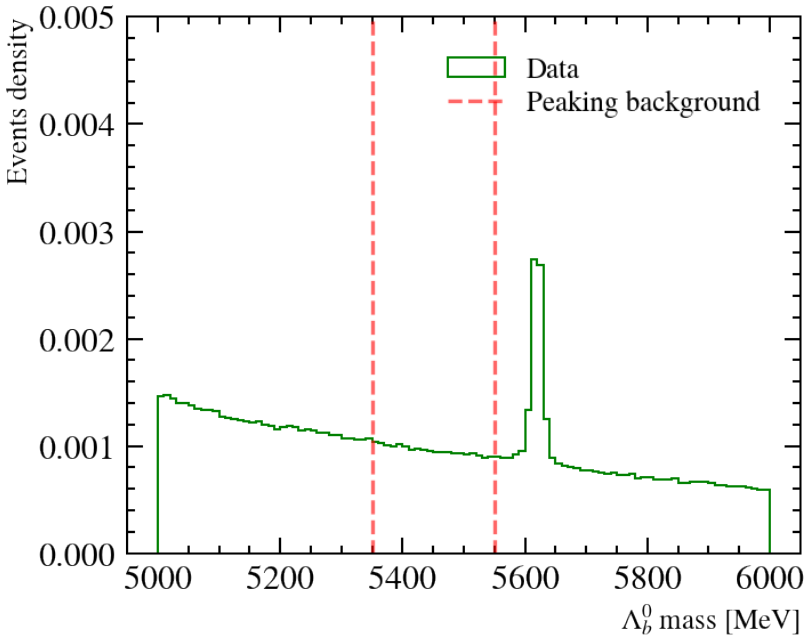

(b) With peaking background cut

Figure 4.3: Normalized Λ_b^0 mass plots with and without the peaking background cut applied.

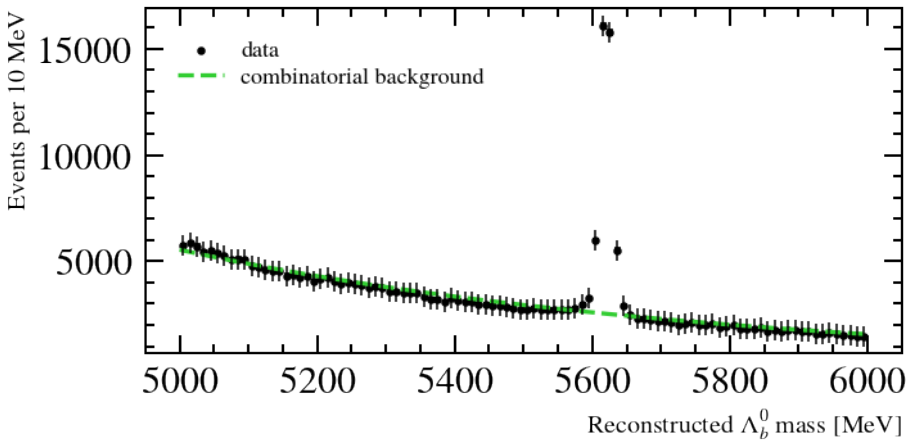

Figure 4.4: Fitting the combinatorial background of the Λ_b^0 mass using an exponential fit function in real data.

4.4 Signal modelling

So far, all of the analysis has been focused on either increasing the resolution, cleaning up the background, or fitting the background of the signal. Entering the phase of analysis of the signal itself, the first step is fitting the Λ_b^0 mass peak using a Crystal Ball function [14]. A Crystal Ball function is composed of a Gaussian distribution to fit the central part of the data which reflects the expected particle mass and the mass resolution of the detector, followed by a power-law tail to account for non-Gaussian effects such as energy loss and detector resolution. To determine the most suitable fit parameters, the fitting was first done on the simulated data to determine the initial parameters. The result of this can be seen in Figure 4.5.

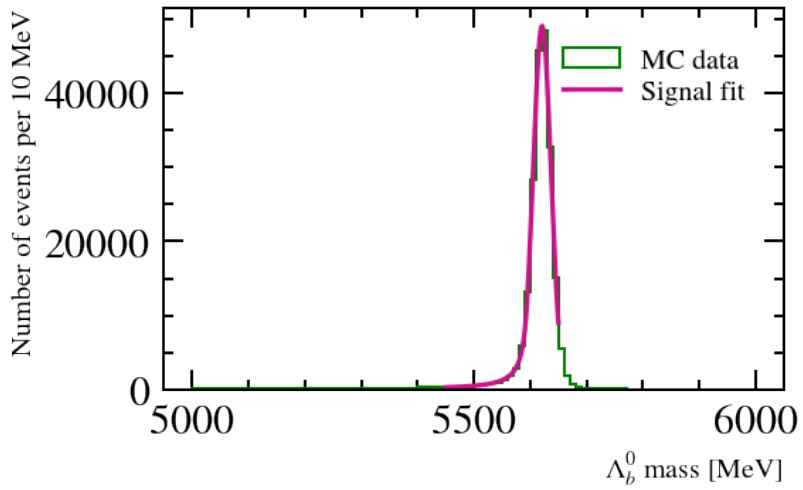

Figure 4.5: Fitting the mass of the Λ_b^0 particle using the Crystal Ball function on simulated data.

These parameters were then transferred to the real data where the last adjustments to the normalization were made. The resulting fit can be seen in Figure 4.6.

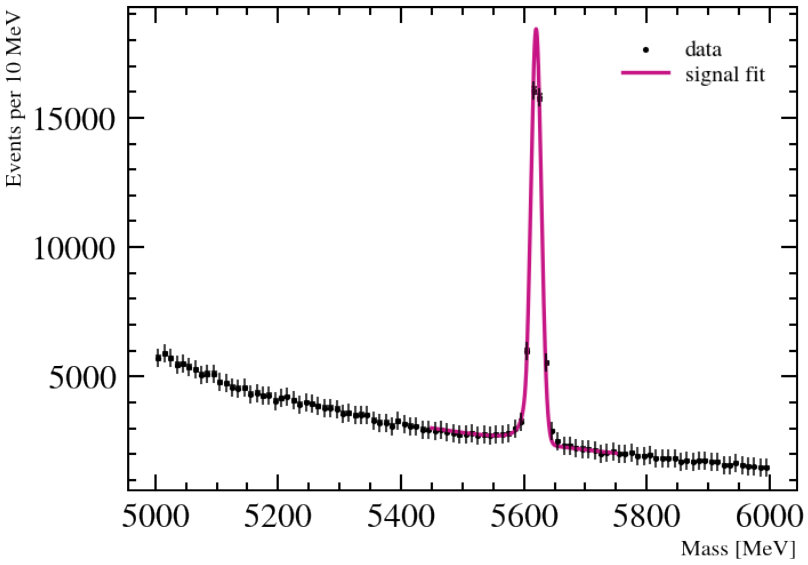

Figure 4.6: Fitting the mass of the Λ_b^0 particle using the Crystal Ball function on real data.

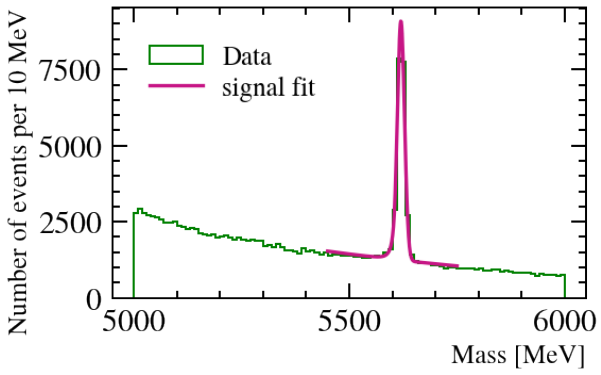

(a) Data with antiparticle selection

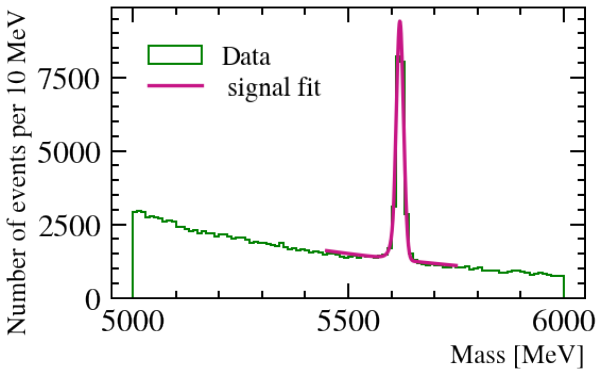

(b) Data with particle selection

Figure 4.7: Λ_b^0 mass plots with selections on particles or antiparticles.

4.5 Particle-antiparticle ratio and final data model

Since the final goal is to count the number of Λ_b^0 particles and $\overline{\Lambda}_b^0$ antiparticles to then draw a ratio between the two, a new selection rule is implemented on the total of the signal according to which, particles and antiparticles can be differentiated. This is achieved by using the secondary decay of $\Lambda_b^0 \to \Lambda^0 J/\psi$, where the Λ^0 particle further decays following the $\Lambda^0 \to p^+\pi^-$ mode. By filtering based on the signs of the proton and pion produced in this mode, the Λ^0 particle can be determined to be either a particle or an antiparticle as shown in Equation 4.6.

$$\begin{aligned} \Lambda_b^0 &\to \Lambda^0 J/\psi \text{ with } \Lambda^0 \to p^+\pi^- \\ \overline{\Lambda}_b^0 &\to \overline{\Lambda}^0 J/\psi \text{ with } \overline{\Lambda}^0 \to p^-\pi^+ \end{aligned} \tag{4.6}$$

The sign of the proton and the pion can be determined from the variables in the branches of the decay tree. Using these variables to select between plotting the Λ^0 or the $\overline{\Lambda}^0$ mass and adjusting the fit normalization to the height of the main peak. Figure 4.7 shows that these two separated data sets look identical in shape.

The counts of the particles and antiparticles can be taken to be the same as the value of the normalization divided by the bin width used to plot the data, given that the Crystal Ball is a probability density function. Using the values of the counts, the ratio is determined by Equation 4.7.

$$\mathcal{A} = \frac{N(\Lambda_b^0) - N(\overline{\Lambda}_b^0)}{N(\Lambda_b^0) + N(\overline{\Lambda}_b^0)} \tag{4.7}$$

The resulting counts as well as the ratio is shown in Table 4.3.

Λ_b^0 count	17700 ± 380
$\overline{\Lambda}_b^0$ count	17000 ± 350
Count ratio	0.020 ± 0.015

Table 4.3: The count of Λ_b^0 and $\overline{\Lambda_b^0}$ as well as their ratio with errors after integrating over the peak using the Crystal Ball fit function

Here, the ratio converted to percentage is $2.0 \pm 1.5\%$ and is taken as the raw asymmetry between the Λ_b^0 particles and the $\overline{\Lambda}_b^0$ antiparticles.

Lastly, adding up all of the individual fit functions for the background as well as the signal, with all of the selection rules apart from the particle-antiparticle selection applied, the result is shown in Figure 4.8.

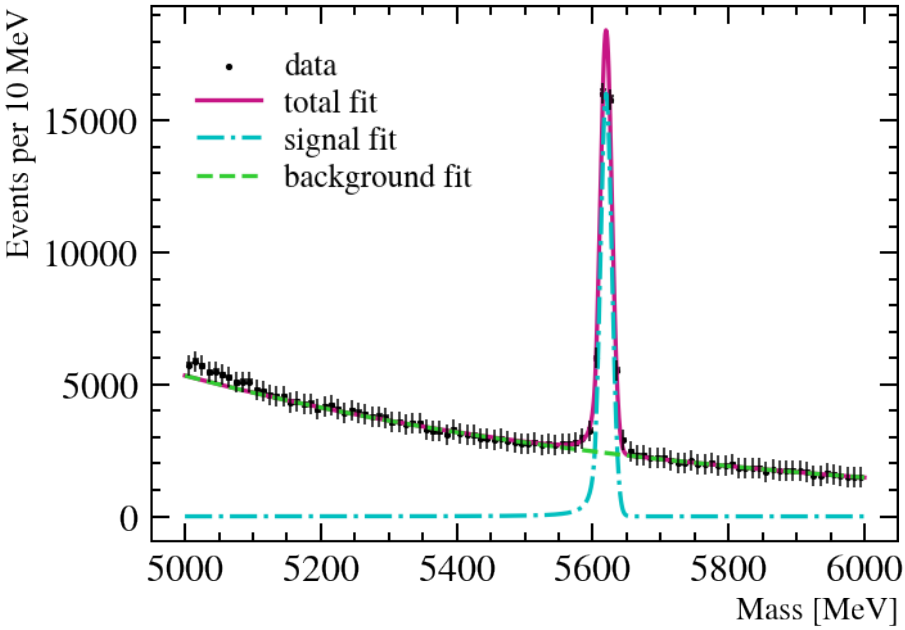

Figure 4.8: Fitting the mass of the Λ_b^0 particle using the Crystal Ball function for the signal and exponential function for the combinatorial background on real data.

5. Discussion

To begin with, it is important to understand, that although several selection rules based on theory as well as statistical arguments are adopted, the choice in ranges remains, to a certain extent, arbitrary and thus impacts the quality of the final results. Similarly, the cuts applied to reduce the peaking background still inevitably hurt the signal and thus reduce the amount of data considered in the final result. Although this latter issue is not as detrimental since this paper focuses more on the ratio of the counts rather than the counts themselves, maximizing signal efficiency is always beneficial in achieving the best results.

5.1 Evaluating results

The goal of this research was to calculate the ratio between the Λ_b^0 particles and $\overline{\Lambda}_b^0$ antiparticles from their respective counts found using the signal fit. For the $\Lambda_b^0 \to \Lambda^0 J/\psi$ decay, as well as its antiparticle version, the theoretical predictions from the SM suggest no asymmetry in their behaviour. Furthermore, for there to be a statistically significant asymmetry that would suggest CP violation or other physics that is beyond the SM, the confidence level needs to be at least 5σ. From the data analysis conducted here, the deduced raw asymmetry is $2.0 \pm 1.5\%$ in favour of particles. This raw asymmetry is statistically insignificant since the confidence level is around 1.3σ, thus no CP violation effects or other beyond the SM effects can be confirmed. This result is consistent with other research [22][23]. To fully determine if there is any CP violation, the asymmetries in the detection process and the production of particles need to be investigated.

5.2 Sources of error and improvement

One of the most important factors to consider when evaluating the validity of the results is how the Λ_b^0 particles and antiparticles were selected. Improvement of the selection of the squared dimuon mass q^2 and the selection of the η ranges is currently not an issue, given that the former is easily determined for decays involving muons and the latter is set by the detector itself. Despite this, adding more variables which could be used to better filter the signal would be highly beneficial. Further selections could be made on variables such as the momentum or the mean lifetime of the Λ_b^0 as well as the Λ particles.

Furthermore, the peaking background produced by the $B^0 \to J/\psi K_s^0$ decay is the next aspect to be considered for improvement. Previously, this report briefly touched upon different strategies which could be used to eliminate this background from the signal, however in the end only one of these strategies was tested and adopted. Applying a cut on the reconstructed K_s^0 mass successfully eliminated the broad peak located left of the Λ_b^0 mass peak with the efficiency of the signal being suffi-

ciently high (82.33%) and the background efficiency being sufficiently low (3.37%). Superficially, this suggests that the approach is satisfactory. In order to improve the treatment of the peaking background more comprehensively, techniques such as using the $2D$ distributions of $m_{K_s^0}$ and $m_{\Lambda_b^0}$, Armenteros-Podolanski plots [24] or machine-learning based techniques that could account for the interdependence of multiple variables, are suggested.

Moving forward, evaluating the various fit functions used to analyse the data is considerably the most relevant aspect of the analysis process. The combinatorial background fit used an exponential function which performed satisfactorily. Despite this, other fit functions such as polynomials of higher degrees could be a better fit and thus need to be investigated. In addition to this, the fitting of the Λ_b^0 mass peak raises concern. Firstly, the choice of using the Crystal Ball function is justified using theory and performed adequately, however, it still remains to be seen if it is the best-fit function to use in this instance. Another option would be to use a double-sided Crystal Ball function, which is better suited to modelling asymmetric peaks than the single-sided Crystal Ball function (used in this research). To continue, the process of the fit parameter determination leaves much to be desired as well. The initial fit parameters were determined using ROOT and then translated into uproot to determine the final fit. The process of finalizing the parametrization in uproot is tedious as well as difficult to qualitatively evaluate. Not only do all the parameters need to be checked among each other, but factors such as effective binning as well as modifying the plotting and fitting ranges play a surprisingly large role in achieving a satisfactory fit. Manually, this process is not efficient time-wise and moreover, complicates the matter of selecting the best fit. Therefore, it is highly necessary to expedite the parametrization process by automating it as well as conducting a more in-depth analysis of the interplay of each parameter. By improving the fit of the Λ_b^0 mass peak, the improvement of the ratio depicting the symmetry between particles and antiparticles follows.

Lastly, there is a need to evaluate systematic errors, which were not investigated at all. These errors arise from detector effects that were not previously considered and can potentially affect Λ_b^0 particles and $\overline{\Lambda}_b^0$ antiparticles differently. One suggested check to screen for this, is analysing the data based on the polarization of the magnet within the detector as well as checking if the luminosity for both such sets of data is comparable.

6. Conclusion

To conclude, the goal of this research is to analyze the $\Lambda_b^0 \to \Lambda^0 J/\psi$ and the $\overline{\Lambda}_b^0 \to \overline{\Lambda}^0 J/\psi$ decays at the LHCb experiment, in order to test matter-antimatter symmetry. The presence of asymmetry in the ratio of the particle and antiparticle counts could suggest the presence of CP violation effects, which are one avenue of research when investigating physics beyond the SM. The data analysis was conducted on the Run 2 data (years 2016 to 2018), using p-p collisions at 13 TeV with a luminosity of 5.4 fb^{-1}. The particle-antiparticle ratio was determined to be $2.0 \pm 1.5\%$, which is taken to be the raw asymmetry. This value is not statistically significant, meaning that no asymmetry was observed. Subsequently, this means that no CP violation effects were detected either. These results are consistent with other such research. To further verify these conclusions, improvements in the selection of Λ_b^0 candidates, the treatment of the peaking background, the signal as well as background modeling, and finally, a thorough investigation of systematic errors are suggested in the previous section. Finally, to fully improve this result, the asymmetries in the detection as well as the particle production processes need to be investigated and quantified.

Bibliography

[1] Python Software Foundation, *Python 3.0 documentation*, Accessed: 2024-09-23, 2008. [Online]. Available: https://docs.python.org/3.0/.

[2] S.-H. Project, *Uproot documentation*, Accessed: 2024-09-23, 2024. [Online]. Available: https://uproot.readthedocs.io/en/latest/.

[3] Wikipedia, *Standard model*, Last accessed 5 September 2024, 2024. [Online]. Available: https://en.wikipedia.org/wiki/File:Standard_Model_of_Elementary_Particles.svg.

[4] LHCb Collaboration, "Measurement of matter–antimatter differences in beauty baryon decays," *Nature Physics*, vol. 13, no. 4, pp. 391–396, Jan. 2017, ISSN: 1745-2481. DOI: 10.1038/nphys4021. [Online]. Available: http://dx.doi.org/10.1038/nphys4021.

[5] N. Cabibbo, "Unitary symmetry and leptonic decays," *Phys. Rev. Lett.*, vol. 10, pp. 531–533, 12 Jun. 1963. DOI: 10.1103/PhysRevLett.10.531. [Online]. Available: https://link.aps.org/doi/10.1103/PhysRevLett.10.531.

[6] M. Kobayashi and T. Maskawa, "CP-Violation in the Renormalizable Theory of Weak Interaction," *Progress of Theoretical Physics*, vol. 49, no. 2, pp. 652–657, Feb. 1973, ISSN: 0033-068X. DOI: 10.1143/PTP.49.652. eprint: https://academic.oup.com/ptp/article-pdf/49/2/652/5257692/49-2-652.pdf. [Online]. Available: https://doi.org/10.1143/PTP.49.652.

[7] S. Navas *et al.*, "Review of particle physics," *Phys. Rev. D*, vol. 110, no. 3, p. 030 001, 2024. DOI: 10.1103/PhysRevD.110.030001.

[8] CERN, *The large hadron collider*, Last accessed 6 September 2024, 2024. [Online]. Available: https://home.cern/science/accelerators/large-hadron-collider.

[9] CERN, *Where did it all begin?* Last accessed 6 September 2024, 2024. [Online]. Available: https://home.cern/about/who-we-are/our-history.

[10] D. Cassidy, "Introduction," in *A Short History of Physics in the American Century*. Cambridge, MA and London, England: Harvard University Press, 2013, pp. 1–5, ISBN: 9780674062740. DOI: doi:10.4159/harvard.9780674062740.intro. [Online]. Available: https://doi.org/10.4159/harvard.9780674062740.intro.

[11] W. A. Fedak and J. J. Prentis, "The 1925 Born and Jordan paper "On quantum mechanics"," *American Journal of Physics*, vol. 77, no. 2, pp. 128–139, Feb. 2009, ISSN: 0002-9505. DOI: 10.1119/1.3009634. eprint: https://pubs.aip.org/aapt/ajp/article-pdf/77/2/128/13086244/128_1_online.pdf. [Online]. Available: https://doi.org/10.1119/1.3009634.

[12] R. Aaij *et al.*, "Design and performance of the LHCb trigger and full real-time reconstruction in Run 2 of the LHC," *JINST*, vol. 14, no. 04, P04013, 2019. DOI: 10.1088/1748-0221/14/04/P04013. arXiv: 1812.10790 [hep-ex].

[13] Y. K. Hsiao and C. Q. Geng, "Direct cp violation in lb decays," *Physical Review D*, vol. 91, no. 11, Jun. 2015, ISSN: 1550-2368. DOI: 10.1103/physrevd.91.116007. [Online]. Available: http://dx.doi.org/10.1103/PhysRevD.91.116007.

[14] R. Aaij and others (LHCb collaboration), "Differential branching fraction and angular analysis of $\Lambda_b^0 \to \Lambda\mu^+\mu^-$ decays," *Journal of High Energy Physics*, vol. 2015, no. 6, p. 115, 2015. DOI: 10.1007/JHEP06(2015)115. [Online]. Available: https://doi.org/10.1007/JHEP06(2015)115.

[15] LHCb Collaboration, *Kaon Mass Calculation Formula in TMath*, https://gitlab.cern.ch/LHCb-RD/ewprlambda/-/blob/master/Studies/background_study/plot_backgrounds_and_signal.py?ref_type=heads#L150, Accessed: 2024-09-08, 2024.

[16] D. S. Pereira, J. Ferraz, F. S. N. Lobo, and J. P. Mimoso, "Baryogenesis: A symmetry breaking in the primordial universe revisited," *Symmetry*, vol. 16, no. 1, p. 13, Dec. 2023, ISSN: 2073-8994. DOI: 10.3390/sym16010013. [Online]. Available: http://dx.doi.org/10.3390/sym16010013.

[17] V. Dedu, *Branching fraction measurment of* $\Lambda_b^0 \to \Lambda^0 J/\psi$, Last accessed 5 September 2024, 2020.

[18] L. Greeven, "Decoding beauty: Rare baryonic decays scifi detector commissioning," English, Ph.D. dissertation, Maastricht University, 2024, ISBN: 9789464960563. DOI: 10.26481/dis.20240403lg.

[19] M. A. Paracha, I. Ahmed, and M. J. Aslam, "Imprints of CP-violation asymmetries in rare Λb → Λ +- decay in a family non-universal Z model," *Progress of Theoretical and Experimental Physics*, vol. 2015, no. 3, 033B04, Mar. 2015, ISSN: 2050-3911. DOI: 10.1093/ptep/ptv017. eprint: https://academic.oup.com/ptep/article-pdf/2015/3/033B04/19301774/ptv017.pdf. [Online]. Available: https://doi.org/10.1093/ptep/ptv017.

[20] LHCb Collaboration, A. A. A. Jr, L. M. A. Filho, *et al.*, "The lhcb detector at the lhc," *Journal of Instrumentation*, vol. 3, no. 08, S08005, Aug. 2008. DOI: 10.1088/1748-0221/3/08/S08005. [Online]. Available: https://dx.doi.org/10.1088/1748-0221/3/08/S08005.

[21] R. Antunes-Nobrega, A. França-Barbosa, I. Bediaga, *et al.*, *LHCb reoptimized detector design and performance: Technical Design Report* (Technical design report. LHCb). Geneva: CERN, 2003. [Online]. Available: https://cds.cern.ch/record/630827.

[22] R. Aaij, B. Adeva, M. Adinolfi, *et al.*, "Observation of the decay λ b 0 →pk - μ + μ - and a search for cp violation," *Journal of High Energy Physics*, vol. 2017, no. 6, Jun. 2017, ISSN: 1029-8479. DOI: 10.1007/jhep06(2017)108. [Online]. Available: http://dx.doi.org/10.1007/JHEP06(2017)108.

[23] R. Aaij, A. S. W. Abdelmotteleb, C. Abellán Beteta, *et al.*, "Observation of a Λ_b^0 - $\overline{\Lambda}_b^0$ production asymmetry in proton-proton collisions at $\sqrt{s} = 7$ and 8 tev," *Journal of High Energy Physics*, vol. 2021, no. 10, Oct. 2021, ISSN: 1029-8479. DOI: 10.1007/jhep10(2021)060. [Online]. Available: http://dx.doi.org/10.1007/JHEP10(2021)060.

[24] P. Baladrón Rodríguez, V. Chobanova, X. Cid Vidal, *et al.*, "Calibration of the momentum scale of a particle physics detector using the armenteros-podolanski plot," *Journal of Instrumentation*, vol. 16, no. 06, P06036, Jun. 2021, ISSN: 1748-0221. DOI: 10.1088/1748-0221/16/06/p06036. [Online]. Available: http://dx.doi.org/10.1088/1748-0221/16/06/P06036.